Two-component off-axis jet model for radio flares of tidal disruption events

Yuri Sato,[1,*] Kohta Murase,[2,3,4,†] Mukul Bhattacharya,[2] Jose Carpio,[5] Mainak Mukhopadhyay,[2] and B. Theodore Zhang[3]

[1]*Department of Physical Sciences, Aoyama Gakuin University, 5-10-1 Fuchinobe, Sagamihara 252-5258, Japan*
[2]*Department of Physics; Department of Astronomy & Astrophysics; Center for Multimessenger Astrophysics, Institute for Gravitation and the Cosmos, The Pennsylvania State University, University Park, PA 16802, USA*
[3]*Center for Gravitational Physics and Quantum Information, Yukawa Institute for Theoretical Physics, Kyoto University, Kyoto, Kyoto 606-8502, Japan*
[4]*School of Natural Sciences, Institute for Advanced Study, Princeton, New Jersey 08540, USA*
[5]*Department of Physics & Astronomy; Nevada Center for Astrophysics, University of Nevada, Las Vegas, NV 89154,*

Recently, radio emission from tidal disruption events (TDEs) has been observed from months to years after the optical discovery. Some of the TDEs including ASASSN-14ae, ASASSN-15oi, AT 2018hyz, and AT 2019dsg are accompanied by the late-time rebrightening phase characterized by a rapid increase in the radio flux. We show that it can be explained by the off-axis two-component jet model, in which the late-time rebrightening arises from the off-axis view of a decelerating narrower jet with an initial Lorentz factor of ~ 10 and a jet opening angle of ~ 0.1 rad, while the early-time radio emission is attributed to the off-axis view of a wider jet component. We also argue that the rate density of jetted TDEs inferred from these events is consistent with the observations.

I. INTRODUCTION

A tidal disruption event (TDE) occurs when a star is torn apart by the tidal forces of a supermassive black hole (SMBH) at sufficiently close approaches [1–3]. TDEs provide rich multiwavelength data in radio, infrared (IR)/optical/ultraviolet (UV), x- and gamma-ray bands, which can be used to study the properties of quiescent galaxies, jets, and the circumnuclear medium (CNM). While thermal emission is believed to arise from the debris of the disrupted star by reprocessing [4–9], details of the mechanism remain unclear. Nonthermal emission has also been observed for some TDEs exhibiting outflows, and radio emission is attributed to synchrotron emission from relativistic electrons accelerated in jets or winds. Future multifrequency radio observations will help us reveal the structure and evolution of the outflows [10–12].

At least some TDEs can launch relativistic jets, as inferred from variable x-ray and subsequent radio emission, and 4 jetted TDEs (Swift J1644+57 [13, 14], Swift J2058+05 [15], Swift J1112-8238 [16] and AT 2022cmc [17]) are known to date. The apparent rate density of jetted TDEs is $\sim 0.03\ \mathrm{Gpc^{-3}yr^{-1}}$ [14, 17], which is only $\lesssim 1\%$ of the total TDE rate density, $\sim 10^{2-3}\ \mathrm{Gpc^{-3}\ yr^{-1}}$ [18]. In addition to these jetted events, a growing sample of optically-detected TDEs exhibit radio afterglows that are consistent with emission from nonrelativistic outflows (see Ref. [11] for a review).

The recent discovery of late-time radio emission from some TDEs (e.g., ASASSN-14ae [19], AT 2018hyz [20], AT 2019azh [21]) and radio rebrightening in some other TDEs (e.g., iPTF16fnl [22], AT 2019dsg [23], ASASSN-15oi [24]) point to outflows that become observable after a significant delay (from a few months to years) since the disruption. In particular, Ref. [25] reported late-time radio brightening in some TDEs on a timescale of $\sim 2-4$ years, where more than half of the sample still shows rising emission in the radio band. These TDEs showed a rapid rise and rebrightening in radio emission at late times with a peak radio luminosity of $\sim 10^{38}-10^{39}$ erg s^{-1}. The underlying mechanism of these delayed radio flares in TDEs is of interest, and the outflows can be either jets [26–31] or winds [32–35].

A relativistic jet launched from a black hole – accretion disk system is expected to be structured, as demonstrated in studies of gamma-ray bursts (GRBs) both theoretically and observationally (see e.g., Refs. [36–42]). Such a structured jet is often modeled as a two-component jet with a relativistic inner component and trans-relativistic outer component, and has been exploited to explain multiwavelength data of afterglows (see e.g., Refs. [43–50]). This model may explain the late radio flares such as the rapid rising part and rebrightening of ASASSN-14ae, ASASSN-15oi, AT 2018hyz, and AT 2019dsg, with luminosities of $\sim 10^{38}-10^{39}$ erg s^{-1}. In this work, we explore the origin of such delayed radio emission from these 4 TDEs and propose a two-component off-axis jet model. We show that this model provides a natural explanation for both the observed radio rebrightening at late times and the earlier radio data without the need for late-time engine activity.

II. ONE-COMPONENT JET MODEL

We first consider the standard one-component jet model viewed off-axis to discuss the rapid rise in the radio flux at late times, considering 4 TDEs, namely ASASSN-14ae, ASASSN-15oi, AT 2018hyz, and AT 2019dsg. The jet has an half-opening angle θ_0, initial Lorentz factor Γ_0, isotropic kinetic energy $\mathcal{E}_k^{\rm iso}$, and viewing angle θ_v mea-

* yuris@phys.aoyama.ac.jp (YS)
† murase@psu.edu (KM)

TABLE I. Parameters used for modeling 4 radio TDEs, ASASSN-14ae, ASASSN-15oi, AT 2018hyz, and AT 2019dsg.

		θ_v [rad]	θ_0 [rad]	$\mathcal{E}_k^{\rm iso}$ [erg]	Γ_0	$n_{\rm ext}$ [cm^{-3}]	w	s	ϵ_B	ϵ_e	f_e
Narrow jet	ASASSN-14ae	1.2	0.11	8.0×10^{54}	10	1.0	1.0	2.6	1.0×10^{-5}	0.1	0.1
	ASASSN-15oi					1.0	0.5	2.5	1.5×10^{-3}	0.2	0.3
	AT 2018hyz					1.0	0.5	2.5	1.5×10^{-3}	0.3	0.3
	AT 2019dsg					3.0	1.0	2.5	1.5×10^{-5}	0.1	0.1
Wide jet	ASASSN-14ae	1.2	0.34	1.0×10^{52}	3	1.0	1.0	2.6	6.0×10^{-5}	0.1	0.1
	ASASSN-15oi					1.0	0.5	2.8	1.0×10^{-4}	0.3	0.3
	AT 2018hyz					1.0	0.5	2.5	6.0×10^{-5}	0.1	0.1
	AT 2019dsg					3.0	1.0	2.8	2.0×10^{-4}	0.1	0.1

sured from the jet axis. As the jet propagates through an external medium with a power-law density profile, $n(r) = n_{\rm ext}(r/r_{\rm ext})^{-w}$ with $r_{\rm ext} = 10^{18}$ cm, external shocks are formed. Focusing on the forward shock, we numerically solve the blast wave radius $r(t)$ and its Lorentz factor $\Gamma(t)$, for an initial radius of 10^{13} cm. This radius is comparable to the tidal disruption radius, and our results are unaffected by the choice of $r(t=0)$.

To obtain the radio light curves, we utilize the afterglow module of AMES (Astrophysical Multimessenger Emission Simulator), following the treatments described in Refs. [41, 51] (see also Ref. [52]). Electrons are assumed to be accelerated via the diffusive shock acceleration mechanism, resulting in an electron injection spectrum ε_e^{-s}, where s is the spectral index. A fraction ϵ_B of the downstream internal energy density of the shocked material is converted to the magnetic field, while a fraction ϵ_e is carried by nonthermal electrons. The electron spectrum is calculated by solving the kinetic equation in the no escape limit, as outlined in Ref. [41], accounting for synchrotron, inverse-Compton, and adiabatic loss processes. For a luminosity distance d_L, considering the equal-arrival-time-surface (EATS), the observed photon flux at time $T = t - t_0$ since the time of discovery (t_0) and at frequency ν is calculated as [41, 53]

$$F_\nu(T) = \frac{1+z}{d_L^2}\int_0^{\theta_0} d\theta\,\sin\theta \int_0^{2\pi} d\phi \frac{r^2|\mu-\beta_{\rm sh}|}{1-\mu\beta_{\rm sh}} \times \frac{1}{\Gamma^2(1-\beta\mu)^2}\frac{j'_{\nu'}}{\alpha_\nu}(1-e^{-\tau_\nu})|_{\hat{t}=(T+t_0)/(1+z)+\mu r/c}, \quad (1)$$

where $\beta_{\rm sh} = \sqrt{1-\Gamma_{\rm sh}^{-2}}$ is the shock velocity and its Lorentz factor is $\Gamma_{\rm sh} \approx \sqrt{2}\Gamma$. The integration variables θ and ϕ are the polar angle ($\theta = 0$ is the jet axis) and azimuthal angle, respectively, and $\mu = \sin\theta\sin\theta_v\cos\phi + \cos\theta\cos\theta_v$. Here, $j'_{\nu'}$ is the comoving emission coefficient, and α_ν is the absorption coefficient in the engine frame (that is dropped when the attenuation is irrelevant). For late-time radio observations, t_0 can be assumed to be negligibly small, which implies that the disk is formed and the jet is launched instantaneously after the tidal disruption occurs at $t = 0$. As we consider delayed radio emission at a significantly later epoch of $T \sim 10^7 - 10^8$ s, the light curves obtained here are not affected.

Radio light curves from our theoretical model are shown with solid lines in Figs 1 (a)-(d), and the model parameters are presented in Table I. Our narrow jet explains a rapid rise in radio bands at the late epoch for all 4 TDEs through relativistic beaming effect if the jet is viewed off-axis [54]. The beaming effect becomes weaker as the jet decelerates, resulting in the rising behavior, and the flux peaks when $\Gamma \sim (\theta_v - \theta_0)^{-1}$, after which the emission asymptotically approaches the on-axis light curve ($\theta_v = 0$: dashed lines in Figs. 1 (a)-(d)) [54]. At $T \sim 10^6 - 10^9$ s, we find that the absorption frequency ν_a, the typical frequency ν_m, and the cooling frequency ν_c are ordered as $\nu_a < \nu_m < \nu_c$[1]. The value of ν_m (ν_a) is larger (smaller) than the radio bands. In the off-axis case, the light curves evolve as $F_\nu \propto T^{(21-8w)/3}$. We adopt $w = 0.5$ for ASASSN-15oi and AT 2018hyz, and $w = 1.0$ for ASASSN-14ae and AT 2019dsg. The radio light curves at late times follow $F_\nu \approx T^{5.7}$ and $\approx T^{4.3}$ for $w = 0.5$ and 1.0, respectively, which are consistent with the observed data. For comparison, the dashed lines in Figs. 1 (a)-(d) show the light curves in the on-axis viewing case, for which the flux decreases at later times.

In the off-axis case, the flux starts with a rising part due to the relativistic beaming effect [54]. The radio data of ASASSN-14ae and AT 2018hyz can be explained with such an off-axis jet (see also Refs. [30, 31, 55]). However, for ASASSN-15oi and AT 2019dsg, the observations for $T \lesssim 10^8$ s shows another declining phase before the radio rebrightening phase. The radio emission from our narrow jet viewed off-axis is inconsistent with the earlier radio data, making it difficult for the one-component jet model to describe all the radio data.

III. TWO-COMPONENT JET MODEL

To mimic a structured jet that is more realistic, we consider a two-component jet model, in which another 'wide jet' is added to the narrow jet described in Sec. II.

[1] Between $\sim 10^6$ s and $\sim 10^9$ s, for ASASSN-14ae and AT 2019dsg, the absorption and typical frequencies are $\nu_a \sim 10^9$ Hz and $\nu_m \sim 10^{10} - 10^{11}$ Hz, respectively. For ASASSN-15oi and AT 2018hyz, the corresponding frequencies are $\nu_a \sim 10^9$ Hz and $\nu_m \sim 10^{12}$ Hz.

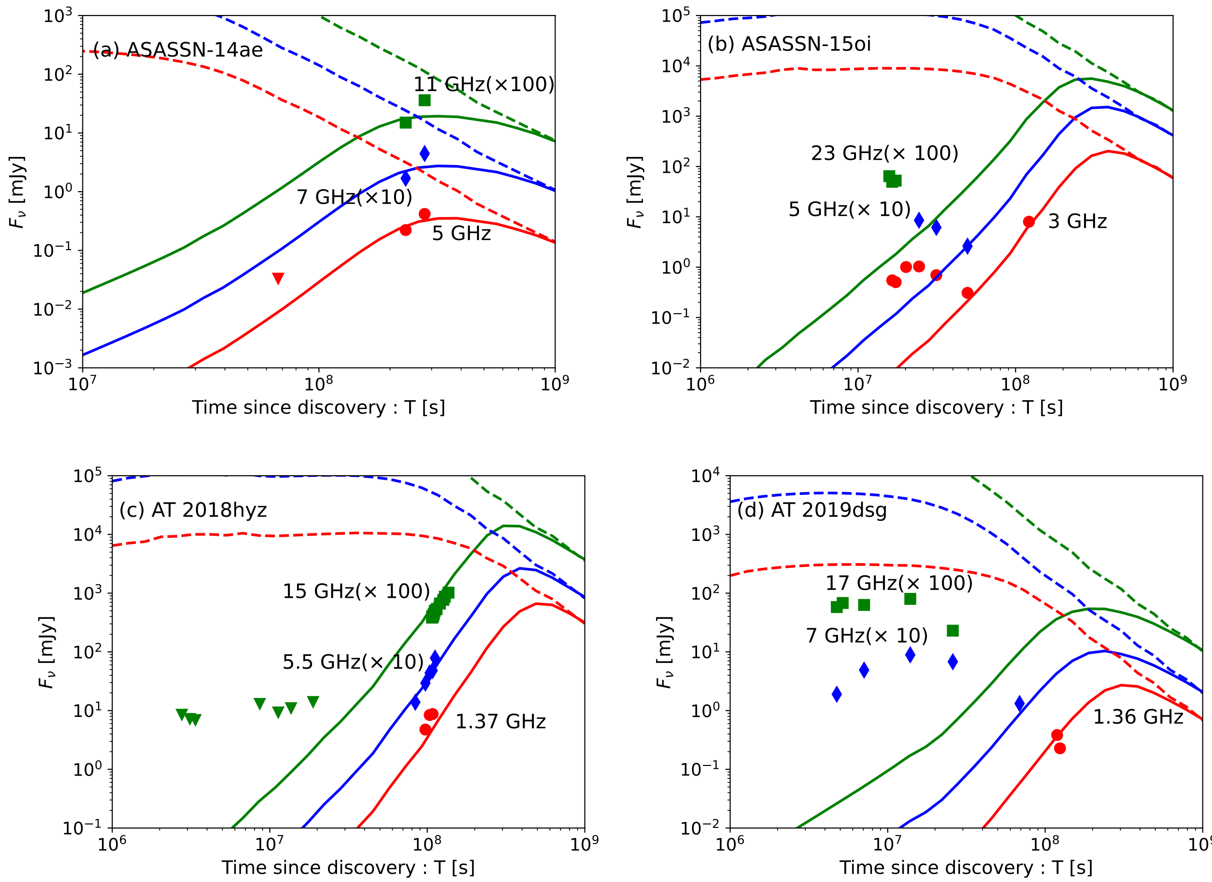

FIG. 1. Observed radio data for ASASSN-14ae (5 GHz: red filled-circles, 7 GHz: blue diamonds, and 11 GHz: green squares) taken from Ref. [25], ASASSN-15oi (3 GHz: red filled-circles, 5 GHz: blue diamonds, and 23 GHz: green squares) obtained from Ref. [24], AT 2018hyz (1.37 GHz: red filled-circles, 5.5 GHz: blue diamonds, and 15 GHz: green squares) extracted from Ref. [20] and AT 2019dsg (1.36 GHz: red filled-circles, 7 GHz: blue diamonds, and 17 GHz: green squares) derived from Refs. [25, 34] are shown. These are compared with the light curves from single jets in the radio bands [ASASSN-14ae; 5 GHz: red, 7 GHz: blue, and 11 GHz: green), ASASSN-15oi (3 GHz: red, 5 GHz: blue, and 23 GHz: green), AT 2018hyz (1.37 GHz: red, 5.5 GHz: blue, and 15 GHz: green) and AT 2019dsg (1.36 GHz: red, 7 GHz: blue, and 17 GHz: green]. The upper limits in radio flux are shown with downward triangles. In all four panels, the solid lines represent the emission from our narrow jet viewed off-axis, and the dashed lines show the results for the on-axis viewing case ($\theta_v = 0$ with other parameters unchanged).

The observed flux is calculated by AMES as a superposition of radio emission from each jet component. We assume that both jet components are launched from the SMBH at the same time and in the same direction. The parameters of both jets are summarized in Table I.

Our values of ϵ_B ($\mathcal{E}_k^{\rm iso}$) are smaller (larger) than the previous works for jetted TDEs [30, 55, 56]. In the on-axis viewing case and the post-jet-break decay phase, the fluxes depend on ϵ_B and $\mathcal{E}_k^{\rm iso}$ as $F_\nu \propto \epsilon_B^{1/3} \mathcal{E}_k^{\rm iso\, 2(5-2w)/3(3-w)}$, for $\nu_a < \nu < \nu_m$. The fluxes in the case of small ϵ_B and large $\mathcal{E}_k^{\rm iso}$ are consistent with the fluxes with large ϵ_B and small $\mathcal{E}_k^{\rm iso}$. For AT 2018hyz, the values of ϵ_B and $\mathcal{E}_k^{\rm iso}$ are adapted from Ref. [31]. Moreover, our parameters for both jets are also consistent with the previous two-component jet scenario [45]. As shown in Fig. 2, the late-time radio data at $T \gtrsim 10^8$ s can be explained by the off-axis narrow jet emission (dashed lines), while the radio emission at $T \lesssim 10^8$ s can be interpreted as the wide jet emission (dotted lines).

ASASSN-15oi and AT 2019dsg have the first radio peaks around $T \sim 2\times10^7$ s and at $T \sim 10^7$ s, respectively. Our wide jet emission provides a viable explanation for the observed radio flux. The wide jet reaches the post-jet-break decay phase from $T \sim 10^6$ s to $T \sim 10^9$ s. When it is assumed that the wide jet enters the post-jet-break decay phase, the observer time of the flux maximum is analytically given by

$$T_{\rm pk} \sim \frac{1+z}{c} \left(\frac{(3-w)\mathcal{E}_k^{\rm iso}\theta_0^2}{4\pi \times 10^{18w} n_{\rm ext} m_p c^2} \right)^{\frac{1}{3-w}} (\theta_v - \theta_0)^2. \quad (2)$$

For our wide jet parameters, we obtain $T_{\rm pk} \sim 9\times10^6$ s for ASASSN-14ae, $T_{\rm pk} \sim 10^7$ s for ASASSN-15oi, $T_{\rm pk} \sim 10^7$ s for AT 2018hyz, and $T_{\rm pk} \sim 6 \times 10^6$ s for AT 2019dsg,

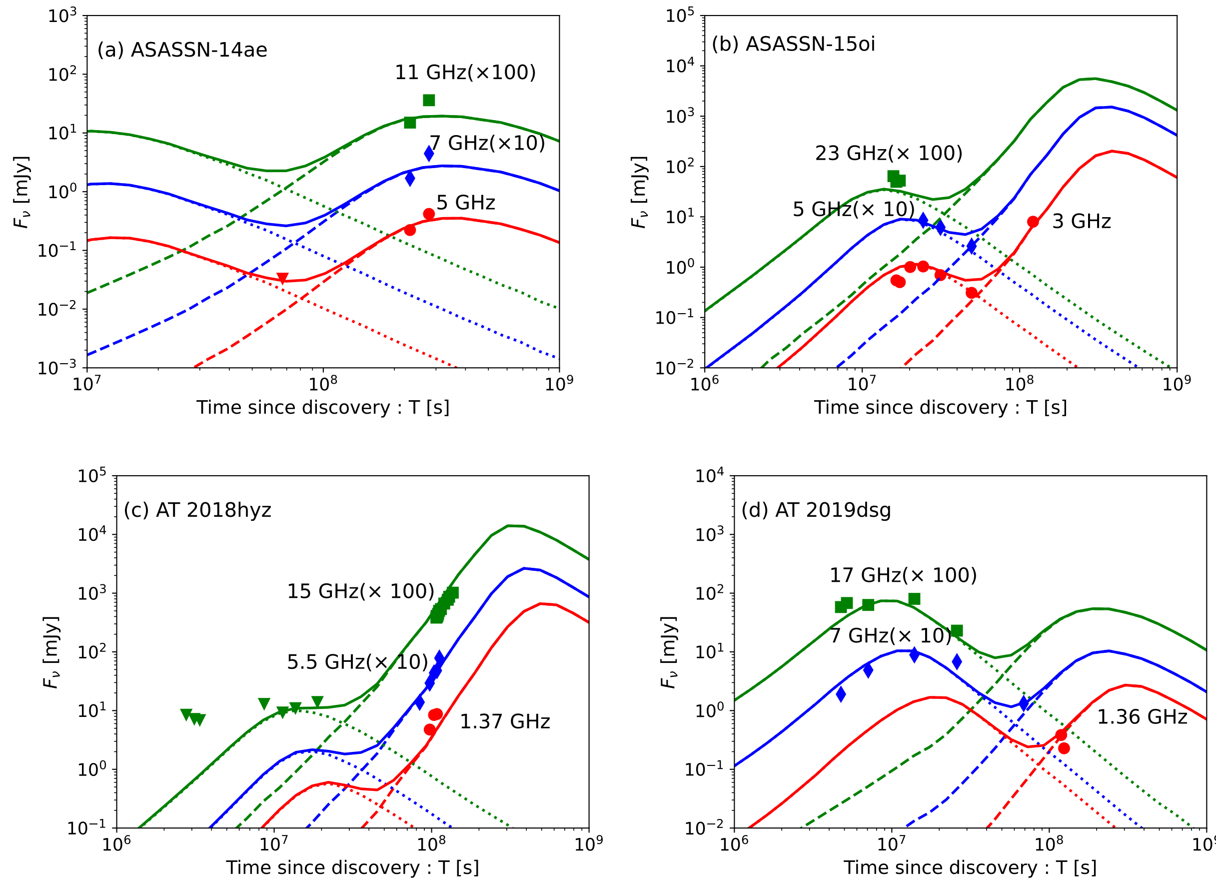

FIG. 2. Radio light curves are calculated with our two-component jet model. The solid lines consist of the sum of emission components of the narrow (dashed lines) and wide (dotted lines) jets. The meanings of colours and observed data are the same as in Fig. 1.

which are consistent with our numerical results within a factor of two. For AT 2018hyz, the value of ϵ_B for the narrow jet is required to be larger than that for the wide jet, so that the second peak is brighter. However, there is parameter degeneracy and this could be attributed to the difference in ϵ_e. The situation is similar for the other 3 TDEs. For example, the second peak of AT 2019dsg can be dimmer for smaller values of ϵ_B and/or ϵ_e. When the properties of CNM and/or jets are different, microphysical parameters may also be different between the narrow and wide jets [47]. More extensive data at multi-wavelengths are required to better estimate the afterglow parameters.

IV. SUMMARY AND DISCUSSION

Radio rebrightening observed from a few TDEs on timescales of several years have been recently reported. Such a long-term rise in the radio band can be explained by either jets or delayed winds. We focused on the former scenario and showed that the two-component off-axis jet model is consistent with the radio data of ASASSN-14ae, ASASSN-15oi, AT 2018hyz, and AT 2019dsg.

Recent studies suggest the importance of structured jets in TDEs, and our results for ASASSN-15oi highlight the limitation of the simplistic one-component jet model, as discussed in Section II and Fig. 1. Interestingly, the radio data consistent with all TDEs may have similar values of $\mathcal{E}_k^{\rm iso}$, Γ_0, and θ_0 (see table I for the parameters used). To explain the rapid rise in the radio light curves, we adopt $w = 0.5,\ 1.0$ as the CNM density profile index. For AT 2019dsg, after 10^8 s, the observed data can be explained by large values of w for the narrow jet. However, from $T \sim 4 \times 10^6$ s to $T \sim 1.2 \times 10^7$ s, the observed light curve at 7 GHz shows the steep rising part of $F_\nu \propto T^4$. Therefore, $w \sim 1$ for our wide jet is favored from the early observational result at 7 GHz [see dotted lines in Fig. 2(d)]. While a density profile with $w = 1.0$ is consistent with that of Sgr A* [57], a shallower density profile with $w = 0.5$ is also reasonable for accretion flows with low viscosity [58]. Moreover, other jetted scenarios [30, 31] also considered the range of $w \lesssim 1$. We note that our model provides qualitative explanations for the radio data. The theoretical fluxes are consistent with the data only within a factor of three, and the two-component jet model would still be too simple to perform quantitative fittings. In addition to such model systematics, parameter degeneracies also exist. Despite these caveats, our modeling favors $w \lesssim 1.0 - 1.5$ for these 4 TDEs showing the steep rising behavior. Analytically, the radio flux in the post-jet-break phase for off-axis viewing is predicted to be $F_\nu \propto T^{(21-8w)/3}$. For $w = 1.5$ that is motivated by the Bondi accretion [59] and $w = 2.5$ that is used for late-time radio emission from some TDEs such as ASASSN-14li [32], we have $F_\nu \propto T^{3.0}$ and $F_\nu \propto T^{0.3}$, respectively (see Sec. II), which are inconsistent with the observed data, especially for ASASSN-15oi and AT 2018hyz.

On-axis jetted TDEs are rarer and brighter with a radio luminosity of $\gtrsim 10^{40}$ erg s^{-1}. As seen from Fig. 2, off-axis narrow jets may have $\sim 10^{39} - 10^{40}$ erg s^{-1} around the peak that is ~ 10 yr after the optical discovery. Although Ref. [25] reported 24 TDEs that are dimmer than on-axis jetted TDEs by $2-3$ orders of magnitude, we expect that off-axis jetted TDEs compose a subdominant population. The apparent rate density of on-axis jetted TDEs is estimated to be $\rho_{\rm jTDE} \approx 0.03^{+0.04}_{-0.02}$ Gpc^{-3}yr^{-1} [60], leading to a true rate density $R_{\rm jTDE} \sim 6$ Gpc^{-3}yr^{-1} of jetted TDEs. The true rate density of jet-loud (or jetted) TDEs including both on-axis and off-axis events is expected to be a few percent of the rate density of all TDEs [60]. Assuming $f_\Omega = (\theta_0 - \theta_v)^2/2 \sim 0.6$ sr as the typical solid angle fraction for off-axis viewing, the expected event rate within $d_L \approx 0.3$ Gpc is estimated to be

$$\begin{aligned} \dot{N}_{\rm jTDE} &\approx \frac{4\pi}{3} d_L^3 R_{\rm jTDE} f_\Omega \\ &\sim 0.4 \ {\rm yr}^{-1} \left(\frac{R_{\rm jTDE}}{6.0 \ {\rm Gpc}^{-3} \ {\rm yr}^{-1}}\right) \left(\frac{d_L}{0.3 \ {\rm Gpc}}\right)^3 \left(\frac{f_\Omega}{0.6 \ {\rm sr}}\right) \end{aligned} \quad (3)$$

This event rate is consistent with radio follow-up observations of optically discovered TDEs for a typical exposure time of $\sim 10^5$ s, a field of view of $\sim 10^{-5} - 10^{-4}$ rad, and a duty cycle of $\sim 0.1 - 1\%$ (see e.g., Refs. [11, 20, 24, 25, 34]). Even with an extreme value of the viewing angle, e.g. $\theta_v \sim \pi/2$, the inferred event rate is not enough to explain the number of radio-detected TDEs, and some other TDEs especially with a radio luminosity of $\sim 10^{37} - 10^{38}$ erg s^{-1} may be explained by delayed disk-driven winds [25].

To reveal the outflow properties of radio-detected TDEs and to go beyond the one-component outflow model, more dedicated observations are necessary. First, samples of radio-detected TDEs are far from complete, and systematic surveys with existing facilities such as VLA (Very Large Array) [61], MeerKAT (South African MeerKAT radio telescope) [62], and ATCA (Australia Telescope Compact Array) [63], and next-generation detectors such as ngVLA (Next Generation Very Large Array) [64] and SKA (Square Kilometre Array) [65] will be useful for detecting more TDEs exhibiting late-time radio rebrightening with $\sim 10^{39} - 10^{40}$ erg s^{-1}. Second, multiyear observations will be crucial for discriminating among different models and modeling the spectral and temporal evolution of radio emission from the outflows. For example, radio emission from AT 2019dsg can also be explained by the wind, so radio data at later times would be useful for testing the off-axis jet model. On the other hand, for ASASSN-14ae and AT 2018hyz, radio data at earlier times would have been beneficial. Third, higher-cadence observations may enable us to identify the peaks and valleys in the predicted light curves, which can also be used for constraining jet properties such as the launching time and Lorentz factor. Note that in this work the jet is assumed to be launched around the disruption time without any significant delay. However, if the disk formation is delayed, the jet launch can also be delayed [66], and afterglow emission may be refreshed by late-time energy injections. Delayed winds and/or jets could also explain some of the radio-detected TDEs [25, 67], although the deceleration may occur at later times.

Multiwavelength observations would be relevant for testing the jet and wind models (Sato et al., in prep). X-ray emission has been detected for some jetted TDEs [13–17], which can be explained by the narrow jet viewed on-axis. While x-ray emission from ASASSN-14ae, ASASSN-15oi, and AT 2018hyz was not observed, AT 2019dsg exhibited x-ray emission that may come from an accretion disk and corona [68]. X-rays from the off-axis jet may be challenging to detect but could be seen by deep observations with *XMM-Newton* (X-ray Multi-Mirror Mission - Newton) [69] and the *Chandra* X-ray Observatory [70] for nearby TDEs and/or with next-generation x-ray telescopes such as *Athena* (Advanced Telescope for the High ENergy Astrophysics) [71] and *eROSITA* (extended Roentgen Survey with an Imaging Telescope Array) [72]. Moreover, quasi-simultaneous optical observations with, e.g., the Vera C. Rubin Observatory [73] will be useful for testing the models.

Multimessenger observations may also provide additional information. Recently, coincident high-energy neutrino events have been reported for several TDEs including AT 2019dsg [23], AT 2019fdr [74], and AT 2019aalc [75]) with a possible time delay of $\sim 150 - 400$ days after their optical discoveries. The on-axis jet model is unlikely for AT 2019dsg [33, 34, 76], and neutrino production in disks [76, 77], coronae [76], winds [76, 78, 79], and choked jets [66, 80, 81] have been considered.

ACKNOWLEDGEMENTS

We thank Kimitake Hayasaki, Tatsuya Matsumoto, Rin Oikawa, Shuta J. Tanaka, and Ryo Yamazaki for valuable comments. This research was partially supported by JSPS KAKENHI, grant numbers 22KJ2643 (YS), 20H01901 and 20H05852 (KM). The work of K.M. is supported by the NSF grants Nos. AST-2108466 and AST-2108467. M.B. acknowledges support from the Eberly Postdoctoral Research Fellowship at the Pennsylvania State University. J.C. is supported by the NSF Grant No. AST-1908689 and No. AST-2108466. J.C. also acknowledges the Nevada Center for Astrophysics and NASA award 80NSSC23M0104 for support. M.M. also acknowledges support from the Institute for Gravitation and the Cosmos (IGC) Postdoctoral Fellowship.

---

[1] J. G. Hills, Possible power source of Seyfert galaxies and QSOs, Nature **254**, 295 (1975).

[2] M. J. Rees, Tidal disruption of stars by black holes of 10 to the 6th-10 to the 8th solar masses in nearby galaxies, Nature **333**, 523 (1988).

[3] C. R. Evans and C. S. Kochanek, The Tidal Disruption of a Star by a Massive Black Hole, Astrophys. J. Lett. **346**, L13 (1989).

[4] A. Loeb and A. Ulmer, Optical appearance of the debris of a star disrupted by a massive black hole, Astrophys. J. **489**, 573 (1997).

[5] L. E. Strubbe and E. Quataert, Optical Flares from the Tidal Disruption of Stars by Massive Black Holes, Mon. Not. Roy. Astron. Soc. **400**, 2070 (2009).

[6] G. Lodato and E. Rossi, Multiband lightcurves of tidal disruption events, Mon. Not. Roy. Astron. Soc. **410**, 359 (2011).

[7] S. Komossa, Tidal disruption of stars by supermassive black holes: Status of observations, JHEAp **7**, 148 (2015).

[8] B. D. Metzger and N. C. Stone, A bright year for tidal disruptions, Mon. Not. Roy. Astron. Soc. **461**, 948 (2016).

[9] N. Roth *et al.*, The X-Ray through Optical Fluxes and Line Strengths of Tidal Disruption Events, Astrophys. J. **827**, 3 (2016).

[10] F. De Colle *et al.*, The dynamics, appearance and demographics of relativistic jets triggered by tidal disruption of stars in quiescent supermassive black holes, Astrophys. J. **760**, 103 (2012).

[11] K. D. Alexander *et al.*, Radio Properties of Tidal Disruption Events, Space Sci. Rev. **216**, 81 (2020).

[12] S. van Velzen *et al.*, Seventeen Tidal Disruption Events from the First Half of ZTF Survey Observations: Entering a New Era of Population Studies, Astrophys. J. **908**, 4 (2021).

[13] J. S. Bloom *et al.*, A relativistic jetted outburst from a massive black hole fed by a tidally disrupted star, Science **333**, 203 (2011).

[14] D. N. Burrows *et al.*, Discovery of the Onset of Rapid Accretion by a Dormant Massive Black Hole, Nature **476**, 421 (2011).

[15] S. B. Cenko *et al.*, Swift J2058.4+0516: Discovery of a Possible Second Relativistic Tidal Disruption Flare, Astrophys. J. **753**, 77 (2012).

[16] G. C. Brown *et al.*, Swift J1112.2−8238: a candidate relativistic tidal disruption flare, Mon. Not. Roy. Astron. Soc. **452**, 4297 (2015).

[17] I. Andreoni *et al.*, A very luminous jet from the disruption of a star by a massive black hole, Nature **612**, 430 (2022), [Erratum: Nature 613, E6 (2023)].

[18] O. Teboul, N. C. Stone, and J. P. Ostriker, Loss cone shielding, Mon. Not. Roy. Astron. Soc. **527**, 3094 (2023).

[19] T. W. S. Holoien *et al.*, ASASSN-14ae: A Tidal Disruption Event at 200 Mpc, Mon. Not. Roy. Astron. Soc. **445**, 3263 (2014).

[20] Y. Cendes *et al.*, A Mildly Relativistic Outflow Launched Two Years after Disruption in Tidal Disruption Event AT2018hyz, Astrophys. J. **938**, 28 (2022).

[21] A. J. Goodwin *et al.*, AT2019azh: an unusually long-lived, radio-bright thermal tidal disruption event, Mon. Not. Roy. Astron. Soc. **511**, 5328 (2022).

[22] A. Horesh *et al.*, Are Delayed Radio Flares Common in Tidal Disruption Events? The Case of the TDE iPTF 16fnl, Astrophys. J. Lett. **920**, L5 (2021).

[23] R. Stein *et al.*, A tidal disruption event coincident with a high-energy neutrino, Nature Astron. **5**, 510 (2021).

[24] A. Horesh, S. B. Cenko, and I. Arcavi, Delayed Radio Flares from a Tidal Disruption Event, Nature Astron. **5**, 491 (2021).

[25] Y. Cendes *et al.*, Ubiquitous Late Radio Emission from Tidal Disruption Events, arXiv e-prints , arXiv:2309.02275 (2023).

[26] D. Giannios and B. D. Metzger, Radio transients from stellar tidal disruption by massive black holes, Mon. Not. Roy. Astron. Soc. **416**, 2102 (2011).

[27] T. Piran *et al.*, "Circularization" vs. Accretion – What Powers Tidal Disruption Events?, Astrophys. J. **806**, 164 (2015).

[28] S. van Velzen *et al.*, A radio jet from the optical and x-ray bright stellar tidal disruption flare ASASSN-14li, Science **351**, 62 (2016).

[29] T. Matsumoto and T. Piran, Generalized equipartition method from an arbitrary viewing angle, Mon. Not. Roy. Astron. Soc. **522**, 4565 (2023).

[30] P. Beniamini, T. Piran, and T. Matsumoto, Swift J1644+57 as an off-axis Jet, Mon. Not. Roy. Astron. Soc. **524**, 1386 (2023).

[31] I. Sfaradi *et al.*, An off-axis relativistic jet seen in the long lasting delayed radio flare of the TDE AT 2018hyz, Mon. Not. Roy. Astron. Soc. **527**, 7672 (2024).

[32] K. D. Alexander *et al.*, Discovery of an outflow from radio observations of the tidal disruption event ASASSN-14li, Astrophys. J. Lett. **819**, L25 (2016).

[33] T. Matsumoto, T. Piran, and J. H. Krolik, What powers the radio emission in TDE AT2019dsg: A long-lived jet or the disruption itself?, Mon. Not. Roy. Astron. Soc. **511**, 5085 (2022).

[34] Y. Cendes *et al.*, Radio Observations of an Ordinary Outflow from the Tidal Disruption Event AT2019dsg, Astrophys. J. **919**, 127 (2021).

[35] K. Hayasaki and R. Yamazaki, Disk Wind–Driven Expanding Radio-emitting Shell in Tidal Disruption Events, Astrophys. J. **954**, 5 (2023).

[36] E. Rossi, D. Lazzati, and M. J. Rees, Afterglow lightcurves, viewing angle and the jet structure of gamma-ray bursts, Mon. Not. Roy. Astron. Soc. **332**, 945 (2002).

[37] B. Zhang and P. Meszaros, Gamma-ray burst beaming: a universal configuration with a standard energy reservoir?, Astrophys. J. **571**, 876 (2002).

[38] K. D. Alexander *et al.*, A Decline in the X-ray through Radio Emission from GW170817 Continues to Support an Off-Axis Structured Jet, Astrophys. J. Lett. **863**, L18 (2018).

[39] K. Ioka and T. Nakamura, Spectral Puzzle of the Off-Axis Gamma-Ray Burst in GW170817, Mon. Not. Roy. Astron. Soc. **487**, 4884 (2019).

[40] O. Gottlieb *et al.*, The structure of weakly magnetized γ-ray burst jets, Mon. Not. Roy. Astron. Soc. **498**, 3320 (2020).

[41] B. T. Zhang *et al.*, The origin of very-high-energy gamma-rays from GRB 221009A: implications for reverse shock proton synchrotron emission, arXiv e-prints , arXiv:2311.13671 (2023).

[42] K. Obayashi *et al.*, GRB 080710: A narrow, structured jet showing a late, achromatic peak in the optical and infrared afterglow?, JHEAp **41**, 1 (2024).

[43] E. Berger *et al.*, A common origin for cosmic explosions inferred from fireball calorimetry, Nature **426**, 154 (2003).

[44] J. L. Racusin *et al.*, GRB 080319B: A Naked-Eye Stellar Blast from the Distant Universe, Nature **455**, 183 (2008).

[45] P. Mimica *et al.*, The radio afterglow of Swift J1644+57 reveals a powerful jet with fast core and slow sheath, Mon. Not. Roy. Astron. Soc. **450**, 2824 (2015).

[46] Y. Sato *et al.*, Off-axis jet scenario for early afterglow emission of low-luminosity gamma-ray burst GRB 190829A, Mon. Not. Roy. Astron. Soc. **504**, 5647 (2021).

[47] Y. Sato *et al.*, Synchrotron self-compton emission in the two-component jet model for gamma-ray bursts, JHEAp **37**, 51 (2023).

[48] Y. Sato *et al.*, Two-component jet model for multi-wavelength afterglow emission of the extremely energetic burst GRB 221009A, Mon. Not. Roy. Astron. Soc. **522**, L56 (2023).

[49] C. Zhou *et al.*, AT2022cmc: A Tidal Disruption Event with a Two-component Jet in a Bondi-profile Circumnuclear Medium, Astrophys. J. **963**, 66 (2024).

[50] O. Teboul and B. D. Metzger, A Unified Theory of Jetted Tidal Disruption Events: From Promptly Escaping Relativistic to Delayed Transrelativistic Jets, Astrophys. J. Lett. **957**, L9 (2023).

[51] B. T. Zhang *et al.*, External Inverse-Compton Emission from Low-luminosity Gamma-Ray Bursts: Application to GRB 190829A, Astrophys. J. **920**, 55 (2021).

[52] K. Murase *et al.*, On the Implications of Late Internal Dissipation for Shallow-Decay Afterglow Emission and Associated High-Energy Gamma-Ray Signals, Astrophys. J. **732**, 77 (2011).

[53] K. Takahashi *et al.*, Probing particle acceleration at trans-relativistic shocks with off-axis gamma-ray burst afterglows, Mon. Not. Roy. Astron. Soc. **517**, 5541 (2022).

[54] J. Granot *et al.*, Off-axis afterglow emission from jetted gamma-ray bursts, Astrophys. J. Lett. **570**, L61 (2002).

[55] T. Matsumoto and B. D. Metzger, Synchrotron afterglow model for AT 2022cmc: jetted tidal disruption event or engine-powered supernova?, Mon. Not. Roy. Astron. Soc. **522**, 4028 (2023).

[56] W.-H. Lei *et al.*, IGR J12580+0134: The First Tidal Disruption Event with an Off-beam Relativistic Jet, Astrophys. J. **816**, 20 (2016).

[57] F. K. Baganoff *et al.*, Chandra x-ray spectroscopic imaging of Sgr A* and the central parsec of the Galaxy, Astrophys. J. **591**, 891 (2003).

[58] I. V. Igumenshchev, M. A. Abramowicz, and R. Narayan, Numerical simulations of convective accretion flows in three dimensions, Astrophys. J. Lett. **537**, L27 (2000).

[59] H. Bondi, On spherically symmetrical accretion, Mon. Not. Roy. Astron. Soc. **112**, 195 (1952).

[60] H. Sun, B. Zhang, and Z. Li, Extragalactic High-energy Transients: Event Rate Densities and Luminosity Functions, Astrophys. J. **812**, 33 (2015).

[61] The official website of VLA, `https://public.nrao.edu/telescopes/vla/`.

[62] The official website of MeerKAT, `https://www.sarao.ac.za/science/meerkat/about-meerkat/`.

[63] The official website of ATCA, `https://www.narrabri.atnf.csiro.au`.

[64] The official website of ngVLA, `https://ngvla.nrao.edu/`.

[65] The official website of SKA, `https://www.skatelescope.org`.

[66] M. Mukhopadhyay, M. Bhattacharya, and K. Murase, Multi-messenger signatures of delayed choked jets in tidal disruption events, arXiv e-prints , arXiv:2309.02275 (2023).

[67] T. Eftekhari *et al.*, Late-time X-ray Observations of the Jetted Tidal Disruption Event AT2022cmc: The Relativistic Jet Shuts Off, arXiv e-prints , arXiv:2404.10036 (2024).

[68] G. Cannizzaro *et al.*, Accretion disc cooling and narrow absorption lines in the tidal disruption event AT 2019dsg, Mon. Not. Roy. Astron. Soc. **504**, 792 (2021).

[69] The official website of *XMM-Newton*, `https://sci.esa.int/web/xmm-newton/`.

[70] The official website of *Chandra*, `https://chandra.harvard.edu`.

[71] The official website of *Athena*, `http://www.the-athena-x-ray-observatory.eu/en`.

[72] The official website of *eROSITA*, `https://www.mpe.mpg.de/eROSITA`.

[73] The official website of Vera C. Rubin Observatory, `https://www.lsst.org`.

[74] S. Reusch *et al.*, Candidate Tidal Disruption Event AT2019fdr Coincident with a High-Energy Neutrino, Phys. Rev. Lett. **128**, 221101 (2022).

[75] S. van Velzen *et al.*, Establishing accretion flares from supermassive black holes as a source of high-energy neutrinos, Mon. Not. Roy. Astron. Soc. **529**, 2559 (2024).

[76] K. Murase *et al.*, High-Energy Neutrino and Gamma-Ray Emission from Tidal Disruption Events, Astrophys. J. **902**, 108 (2020).

[77] K. Hayasaki and R. Yamazaki, Neutrino Emissions from Tidal Disruption Remnants, Astrophys. J. **886**, 114 (2019).

[78] W. Winter and C. Lunardini, A concordance scenario for the observed neutrino from a tidal disruption event, Nature Astron. **5**, 472 (2021).

[79] C. Yuan, W. Winter, and C. Lunardini, AT2021lwx: Another Neutrino-Coincident Tidal Disruption Event with a Strong Dust Echo?, arXiv e-prints , arXiv:2401.09320 (2024).

[80] X.-Y. Wang and R.-Y. Liu, Tidal disruption jets of supermassive black holes as hidden sources of cosmic rays: explaining the IceCube TeV-PeV neutrinos, Phys. Rev. D **93**, 083005 (2016).

[81] N. Senno, K. Murase, and P. Meszaros, High-energy Neutrino Flares from X-Ray Bright and Dark Tidal Disruption Events, Astrophys. J. **838**, 3 (2017).